

Chapter 11

Biological Systems: Multiscale Modeling Based on Mixture Theory

Yusheng Feng, Sarah J. Boukhris, Rakesh Ranjan and Raul A. Valencia

Abstract Scientific understanding of complex biological systems has recently benefited from mathematical and computational modeling. Classical biological studies are focused on observation and experimentation. However, mathematical modeling and computer simulation can provide useful guidance and insightful interpretations for experimental studies. Mathematical modeling can also be used to characterize complex biological phenomena, such as cell migration, cancer metastasis, tumor growth, bone remodeling, and wound healing. Since these phenomena occur over varying spatial and temporal scales, it is necessary to use multiscale modeling approaches. This book chapter provides an overview of multiscale mathematical methods for developing models for aforementioned biological phenomena based on so-called mixture theory. In Sect. 11.1, we cover the background about multiscale modeling in general applications as well as biology specific applications, Sect. 11.2 presents the multiscale computational methods and the challenges associated with modeling complex biological systems and processes, Sect. 11.3 presents theories and their applications of four example model problems, and Sect. 11.4 concludes with open questions in multiscale mathematical modeling, especially in biomedical areas.

11.1 Background

Although microscale and nanoscale systems are becoming more prevalent in many engineering and biological applications, our ability to create predictive and informative mathematical models of these systems is limited [1]. For systems that cannot

Y. Feng (✉) · S.J. Boukhris · R. Ranjan · R.A. Valencia
The University of Texas at San Antonio, One UTSA Circle San Antonio,
TX 78249, USA
e-mail: yusheng.feng@utsa.edu

S.J. Boukhris
e-mail: bcr625@my.utsa.edu

R. Ranjan
e-mail: rakesh.ranjan@utsa.edu

R.A. Valencia
e-mail: raul.valencia@upb.edu.co

© Springer-Verlag London 2015
S. De et al. (eds.), *Multiscale Modeling in Biomechanics
and Mechanobiology*, DOI 10.1007/978-1-4471-6599-6_11

be modeled by continuum or molecular methods alone (e.g., too small or too large), multiscale methods can be implemented. Multiscale methods involve the use of information at various scales, which requires mathematics and computation to simulate a physical or biological system at more than one scale [1]. These methods are mainly divided into two types of approaches: hierarchical and concurrent. The hierarchical approach to multiscale modeling directly uses the information at small length scales and inputs it into larger length scales via an averaging process. The more popular concurrent multiscale methods, in contrast, utilize information at differing scales simultaneously.

Multiscale modeling techniques have relevant uses in many fields of study such as engineering and biology. Materials science has benefited from multiscale methods in the realm of solid mechanics. Studying fluid flow effects in microfluidic devices requires analysis at two or more spatial and temporal scales with coupled chemistry, electrochemistry, and fluid motion [1].

For decades, advances in biology had little to do with contribution from sophisticated mathematical modeling. Biology was mainly based on observation and experimentation and it was not possible to simulate large complex systems. However, now in the age of computers and seemingly endless computational capabilities, there is an avenue for collaboration among biologists, mathematicians, and computational scientists to establish relevant models based on experiments. No longer are there strict limitations in tools and resources to examine life at many scales, which represents the difficulty in modeling biology. It is well known that biological systems are complicated to mathematically model because they involve many interrelated processes across many scales [2]. Each scale level in a biological system, both temporal and spatial, contains information from levels either above or below [3]. The general hierarchy of scales in biological systems follows the order of atom, molecule, macromolecule, organelle, cell, tissue, organ, individual, to population. These complex scales have also been broken up into specific fields of study (i.e., molecular biology, cellular biology, organism studies, and population studies).

In the field of cancer research, the ultimate goal of mathematical modeling and simulation is to aid in development of personalized therapies thereby decreasing patient suffering while increasing treatment effectiveness [4]. Mathematical and computational models, therefore, are needed to quantify the links between 3D tumors and migration, invasion, proliferation, and microscale cellular and environmental characteristics [4]. This task is best accomplished using multiscale methods.

11.2 Multiscale Computational Methods and Challenges

Multiscale methods are specially geared to develop models that are capable of linking molecular, cellular, and tissue continuum scales. The common approach taken in constructing a mathematical model is to begin with a simple model. This model will preserve enough biology to be meaningful, but will include less parameters [3] as to not over complicate the modeling process. The advantage of this approach is that the model can be applied to understand many different biological systems.

A mathematical model that incorporates multiple scales can serve at least two purposes: (1) when detailed information about the biological system is known, the model can be used to conduct *in silico* experiments in lieu of *in vitro* or *in vivo* experiments; and (2) when details are unknown, the model can serve as a tool to test a hypothesis and create a prediction. Extensions and complications can be included into the mathematical model, in the form of additional parameters, to better resemble the biological system [3]. However, it is necessary to avoid overcomplicating the model.

The ultimate goal of multiscale mathematical modeling is to couple discrete particle methods (e.g., molecular dynamics) with models at the continuum level. However, coupling of these two methods is difficult because of the interaction between the interfaces between molecular dynamics and continuum regions. When applying the energy-conservation formulation, this discrepancy is amplified by causing heat generation in the molecular dynamics regime thereby polluting the solution. Another issue in coupling molecular dynamics and continuum methods is in connecting timescales in each region. Several researchers have developed multiscale methods to account for these issues to efficaciously bridge between temporal and spatial scales. The following is a brief overview of commonly used multiscale modeling approaches in the literature.

11.2.1 Bridging Scale Method

The bridging scale method is a concurrent multiscale method that couples the atomistic and continuum simulation methods [1]. The feature of this method is that it is general and can be used in a full three-dimensional domain. At its basic level, the bridging scale method includes the numerical calculation of the time history kernel in multiple dimension so that a two-way coupled coarse and fine molecular dynamics boundary condition is determined. This approach is particularly suitable for dynamics systems with finite temperature.

11.2.2 Bridging Domain Method

The bridging domain method uses molecular dynamics in localized regions then couples it with a continuum region that surrounds the atomistic region [5, 6]. A spatial region contains overlapping continuum and atomistic regions which is best demonstrated by two-dimensional wave and crack propagation scenarios [1].

11.2.3 Quasi-Continuum Method

Using the Cauchy-Born rule [7], which assumes that the continuum energy density can be estimated using an atomistic potential, the analysis at the atomic level is

coupled to the continuum in the Quasi-Continuum method [8]. This approach is similar to an adaptive finite element method [9] which requires that the restriction that the deformation of the lattice of continuum point must be homogeneous.

11.2.4 Coupled Atomistics and Discrete Dislocation

Coupled atomistics and discrete dislocation (CADD) is a method for quasi-static coupling [1]. This approach to multiscale modeling couples molecular statics with discrete dislocation plasticity [10–12], thus making it an especially useful tool in fracture mechanics. Defects such as dislocations generated within the atomistic region pass through to the continuum region where they are characterized by discrete dislocation mechanics [1, 13].

11.2.5 Macroscopic, Atomistic, ab Initio Dynamics

The macroscopic, atomistic, ab initio dynamics (MAAD) multiscale method concurrently links tight binding, molecular dynamics, and finite element methods [14]. All three methods are computed simultaneously and dynamically share and receive information. The approach decreases the mesh size of the finite element mesh until it is on the order of the atomic spacing. Atomic dynamic are then governed by molecular dynamics, then tight binding is used to simulate the atomic bond breaking processes at an area of interest such as a crack tip [1].

11.2.6 Course-Grained Molecular Dynamics

Coarse-grained molecular dynamics (CGMD) is a multiscale approach similar to MAAD but instead couples only finite element and molecular dynamics [15]. It is possible to eliminate the tight binding analysis because the coarse-grained energy approximation converges to the exact atomic energy that is used to derive the governing equations of motion [1].

11.3 Theories and Applications

11.3.1 Multiscale Cell Migration Simulation

Biological studies indicate that abnormal gene mutations in healthy cells may disrupt their regulatory mechanisms that control growth, proliferation, and apoptosis [16]. The uncontrolled growth of these cancer cells creates an avascular tumor mass [17].

Avascular tumors receive nutrients and oxygen via diffusion from nearby vessels [16], but as the tumor grows the demand for nutrients and oxygen increases. When the tumor reaches a critical size, a small amount of cancer cells within the core of the tumor will become necrotic due to the limited nutrient and oxygen supply from diffusion thus initiating cell responses to hypoxia and inducing angiogenesis [18]. The now vascularized tumor creates a pathway that allows for the tumor cells to migrate out of the primary tumor. These circulating tumor cells have the ability to be deposited at a distant site and proliferate to produce secondary tumors [18]. Unfortunately, it is difficult to clinically treat patients with metastatic cancer, in part, because of our limited understanding of the mechanisms of cancer metastasis. Therefore, it is in both scientific and practical healthcare interests to study cell migration and nanoparticle transport in living tissues. However, it is very challenging to quantify cellular motion and nanoparticle transport in an *in vivo* environment. Mathematical and computational models may provide insight into mechanisms that govern the mass transport and cell migration and possibly identify major influencing factors in the process. We introduce a multiscale approach to simulate a simple system that consists of a single fluid channel surrounded by hydrogel matrix with porous structure, which reflects an *in vitro* 3D cell culture apparatus [16]. Cancer cells, nanoparticles, and nutrients are immersed in the fluid, which mimics particle transport in a blood vessel or a lymphatic vessel. The current model considers three kinds of particle mass (cells, nanoparticles, and nutrients) transport driven by the flow inside a channel.

Transport of biochemical species and cellular microfluidics depends on the velocity of the carrier flow and on the size and nature of the biological species [19]. Mass transport can be divided into two types in the circulatory system: (1) transport dominated by convection and (2) transport dominated by diffusion. In the first type of mass transport, cell and nutrient transport within the human vasculature is governed by the local haemodynamics (macro-scale). The second type is the transport within the wall of both the artery and vascular graft (micro-scale). Properties such as permeability, porosity, tortuosity, and diffusivity define how mass are transported within vessel walls. In order to accurately model mass transport through a vessel wall, it is necessary to understand the micro-structure of the wall [20].

It is important to analyze different length and timescales, since, specific consideration may apply at the macro-scale but not at the micro-scale. Usually, the fluid flows by pressure gradient effects and sometimes by electric forces (electro-osmotic flow) at micro-scale. The Knudsen number is useful for determining whether continuum mechanics or statistical mechanics formulation of fluid dynamics should be used [19].

Different physicochemical phenomena of the blood flow and cell migration are associated at different time and length scales. Some of these phenomena are consumption and transport of oxygen and nutrients, osmosis, generation of waste by cells, mechanical loading of cells, electrochemical, chemo-mechanical, and electro-mechanical phenomena, among others. For example, the time for cell synthesis is about weeks while the cell adhesion is about hours. In the same way, the length scale of the hydrogel is about millimeters, while the length of adhesion points of cells is about a few nanometers [21].

11.3.1.1 Mathematical Formulation

The coupling with hydrodynamics consists of a system with five unknown variables: velocity (u, v, w), pressure (p), and concentration (c). The known parameters are the fluid density (ρ), fluid dynamic viscosity (μ), the diffusion constant of the species D , and two external actions on the fluid: the body force per unit volume F and the concentration source or sink per unit volume S . At the macro-scale, the system considers the Navier-Stokes equation and convection-diffusion equation.

$$\frac{\partial \rho}{\partial t} + \nabla \cdot (\rho \mathbf{U}) = 0 \quad (11.1)$$

$$\rho \frac{\partial \mathbf{U}}{\partial t} + \rho \mathbf{U} \cdot \nabla \mathbf{U} = -\nabla p + \mu \Delta \mathbf{U} + \mathbf{F} \quad (11.2)$$

$$\frac{\partial c}{\partial t} + \mathbf{U} \cdot \nabla c = \nabla \cdot (D \nabla c) + S \quad (11.3)$$

The system is under the condition that the concentration of nutrients is sufficiently small as to not affect the carrier fluid viscosity and density. Usually in a microfluidics system, the flow of the carrier fluid is assumed to be steady state and only the nutrient concentration changes with time. In such case, parameters ρ , μ , and D are constant, there is no cell growth ($S = 0$) and there are no body forces (gravity is negligible in very small systems), the system would thus become:

$$\nabla \cdot \mathbf{U} = 0 \quad (11.4)$$

$$\mathbf{U} \cdot \nabla \mathbf{U} = -\frac{1}{\rho} \nabla p + \nu \Delta \mathbf{U} \quad (11.5)$$

$$\frac{\partial c}{\partial t} + \mathbf{U} \cdot \nabla c = D \Delta c \quad (11.6)$$

where ν is the kinematic viscosity. At the macro-scale level, fluid flow through the porous hydrogel matrix is described by the Brinkman equation:

$$\nabla \cdot \mathbf{U} = 0 \quad (11.7)$$

$$\frac{\rho}{\varepsilon} \left[\frac{\partial \mathbf{U}}{\partial t} + (\mathbf{U} \cdot \nabla) \frac{\mathbf{U}}{\varepsilon} \right] = -\nabla p + \nabla \cdot \frac{\mu}{\varepsilon} [\nabla \mathbf{U} + (\nabla \mathbf{U})^T] - \frac{\bar{\mu}}{k} \mathbf{U} + \mathbf{F} \quad (11.8)$$

where ε is the porosity, μ is the dynamic viscosity, $\bar{\mu}$ is the effective viscosity of the medium, and k is the permeability of the media. One approach to calculating the local permeability is the Kozeny-Carman equation below, which relates the porosity to the permeability of the structure [22]:

$$k = \frac{r^2 \varepsilon^3}{4k_k(1 - \varepsilon)^2} \quad (11.9)$$

where r the radius of the cylinders, k_k is the Kozeny-Carman constant, and ε is the porosity of the structure. Kozeny calculated an approximate value of 2 for k_k and Carman suggested a value of 5 based on experimental evidence on an assumed isotropic medium [23].

For the effective viscosity of the medium, Brinkman simply took [21]:

$$\bar{\mu} = \mu \quad (11.10)$$

while Seyam et al. took [24]:

$$\frac{\bar{\mu}}{\mu} = \frac{1}{\varepsilon} \tau \quad (11.11)$$

with τ as the tortuosity of the medium defined below. For the case of this model, we consider Brinkman's simplification to the effective viscosity of a medium.

$$\tau = \sqrt{\varepsilon} \quad (11.12)$$

If the hypothesis of a creeping flow is valid at micro-scale, the system collapses to the linear system [19]:

$$\nabla \cdot \mathbf{U} = 0 \quad (11.13)$$

$$\nabla p = \nu \Delta \mathbf{U} \quad (11.14)$$

The cell motion was tracked using the Newtonian formulation:

$$\frac{d}{dt}(m_p v_p) = F_D + F_g + F_{ext} \quad (11.15)$$

F_D is the drag force from the fluid, which is described as:

$$\mathbf{F}_D = m_p F_d (\mathbf{U} - \mathbf{v}_p) \quad (11.16)$$

where m_p is the individual cell mass and F_d is the drag force per unit mass on the cell. Assuming that the cells take spherical shape, F_d is defined as:

$$F_d = \frac{18\mu}{\rho_p d_p^2} \quad (11.17)$$

where ρ_p is the cell mass density and d_p is the cell diameter. The gravity force F_g is usually negligible in very small systems and F_{ext} is defined as:

$$F_{ext} = M \nabla c - K \mathbf{v}_p \quad (11.18)$$

The first term on the right side, $M\nabla c$, is the attraction to nutrients (based on chemotaxis) and the second term, Kv_p , is the drag force exerted by the porous media. M [$\text{J m}^3/\text{mol}$] and K [N s/m] are two constants that will be determined experimentally. The shear stress for laminar flow of a Newtonian fluid is linearly related to the shear rate (dV/dr) in terms of cylindrical coordinates [25, 26]:

$$\tau = -\mu \frac{dV}{dr} \quad (11.19)$$

where V is the velocity [m/s] at radial position r [m] and μ [N s/m^2] is the dynamic viscosity of the fluid. Wall shear stress for turbulent flow is large compared to laminar flow. For either case, laminar or turbulent, the wall shear stress can be determined from:

$$\tau = -\frac{d \Delta p}{4 L} \quad (11.20)$$

Wall shear stress of Newtonian fluids in tubular vessels can be calculated as a function of volumetric flow rate:

$$\tau = \frac{4\mu Q}{\pi r^3} \quad (11.21)$$

based on Hagen-Poiseuille equation:

$$\Delta p = 128 \frac{\mu L Q}{\pi d^4} \quad (11.22)$$

The diffusion constant in the fluid for nutrients was estimated by the Stokes-Einstein diffusivity equation for diffusion of spherical particles through liquid with a low Reynolds number [20, 27]:

$$D = \frac{k_B T}{6 \pi \mu r} \quad (11.23)$$

where k_B is the Boltzmann's Constant, T is the absolute temperature and r is the radius of the spherical particles. r was estimated from the assumed molecular weight and the following equation for a sphere:

$$r = \left(\frac{3 \cdot M_w \cdot V_p}{4 \pi N_A} \right)^{\frac{1}{3}} \quad (11.24)$$

where V_p is the molecule's specific volume, M_w is the molecular weight, and N_A is Avogadro's number. The characteristic Knudsen Number (Kn) is defined as [19]:

$$Kn = \frac{\lambda}{L} \quad (11.25)$$

where λ is the mean free path of the molecules and L is the characteristic dimension of the channel.

Weak Formulation

For this study, fluid was assumed to be Newtonian, homogeneous, and incompressible. The equations solved were:

$$\nabla \cdot \sigma = \rho(\mathbf{u} \cdot \nabla \mathbf{u}) \text{ in } \Omega \quad (11.26)$$

$$\nabla \cdot \mathbf{u} = 0 \quad \text{in } \Omega \quad (11.27)$$

Given the strong form, the boundary conditions and weak form can be described as follows:

$$\mathbf{u} = \tilde{\mathbf{u}} \quad \text{on } \Gamma_D \quad (11.28)$$

$$\sigma \cdot \mathbf{n} = \tilde{\mathbf{h}} \quad \text{on } \Gamma_N \quad (11.29)$$

The weak form is obtained by taking the scalar product of the momentum equations with a vector test function \mathbf{v} belonging to a functional space $\mathbf{V} = \{\mathbf{v} | \mathbf{v} \in \mathbf{H}^1(\Omega), \mathbf{v}|_{\Gamma_D} = 0\}$, integrating over Ω and applying the Green integration formula.

Similarly, the continuity equation is operated by multiplying by a function $q \in \mathbf{Q} = \{q | q \in \mathbf{H}^1(\Omega)\}$.

$$\int_{\Omega} (\nabla \cdot \sigma) \cdot \mathbf{v} d\Omega - \int_{\Omega} \rho(\mathbf{u} \cdot \nabla \mathbf{u}) \cdot \mathbf{v} d\Omega = 0 \quad (11.30)$$

$$\int_{\Omega} (\nabla \cdot \mathbf{u}) \mathbf{q} d\Omega = 0 \quad (11.31)$$

Substituting the identity $(\nabla \cdot \sigma) \cdot \mathbf{v} = \nabla \cdot (\sigma \cdot \mathbf{v}) - \sigma : \nabla \mathbf{v}$:

$$\int_{\Omega} (\nabla \cdot \sigma) \cdot \mathbf{v} d\Omega = \int_{\Omega} (\nabla \cdot (\sigma \cdot \mathbf{v}) - \sigma : \nabla \mathbf{v}) d\Omega \quad (11.32)$$

$$\int_{\Omega} (\nabla \cdot \sigma) \cdot \mathbf{v} d\Omega = \int_{\Omega} \nabla \cdot (\sigma \cdot \mathbf{v}) d\Omega - \int_{\Omega} \sigma : \nabla \mathbf{v} d\Omega \quad (11.33)$$

Applying Green integration:

$$\int_{\Omega} (\nabla \cdot \sigma) \cdot \mathbf{v} d\Omega = \int_{\Gamma} (\sigma \cdot \mathbf{v}) \cdot \mathbf{n} d\Gamma - \int_{\Omega} \sigma : \nabla \mathbf{v} d\Omega \quad (11.34)$$

Applying $(\sigma \cdot \mathbf{v}) \cdot \mathbf{n} = (\sigma \cdot \mathbf{n}) \cdot \mathbf{v}$ due to σ is a symmetric tensor:

$$\int_{\Omega} (\nabla \cdot \sigma) \cdot \mathbf{v} d\Omega = \int_{\Gamma} (\sigma \cdot \mathbf{n}) \cdot \mathbf{v} d\Gamma - \int_{\Omega} \sigma : \nabla \mathbf{v} d\Omega \quad (11.35)$$

Substituting:

$$\int_{\Gamma} (\sigma \cdot \mathbf{n}) \cdot \mathbf{v} d\Gamma - \int_{\Omega} \sigma : \nabla \mathbf{v} d\Omega - \int_{\Omega} \rho(\mathbf{u} \cdot \nabla \mathbf{u}) \cdot \mathbf{v} d\Omega = 0 \quad (11.36)$$

Taking the first term and applying the boundary conditions:

$$\int_{\Gamma} (\sigma \cdot \mathbf{n}) \cdot \mathbf{v} d\Gamma = \int_{\Gamma} \tilde{\mathbf{h}} \cdot \mathbf{v} d\Gamma \quad (11.37)$$

we can organize the weak formulation as

$$\int_{\Gamma_N} \tilde{\mathbf{h}} \cdot \mathbf{v} d\Gamma_N - \int_{\Omega} \sigma : \nabla \mathbf{v} d\Omega - \int_{\Omega} \rho(\mathbf{u} \cdot \nabla \mathbf{u}) \cdot \mathbf{v} d\Omega = 0 \quad (11.38)$$

Based on Newtonian fluid, substituting $\sigma = -p\mathbf{I} + 2\mu\mathbf{D}$:

$$\int_{\Gamma_N} \tilde{\mathbf{h}} \cdot \mathbf{v} d\Gamma_N - \int_{\Omega} (-p\mathbf{I} + 2\mu\mathbf{D}) : \nabla \mathbf{v} d\Omega - \int_{\Omega} \rho(\mathbf{u} \cdot \nabla \mathbf{u}) \cdot \mathbf{v} d\Omega = 0 \quad (11.39)$$

Finally, the weak form reads: Find $u \in V_g = \{u \in H^1(\Omega), u|_{\Gamma_D} = \tilde{u}\}$ and $p \in P = \{p|p \in H^1(\Omega)\}$ such that

$$\int_{\Omega} (-p\mathbf{I} + 2\mu\mathbf{D}) : \nabla \mathbf{v} d\Omega + \int_{\Omega} \rho(\mathbf{u} \cdot \nabla \mathbf{u}) \cdot \mathbf{v} d\Omega = \int_{\Gamma_N} \tilde{\mathbf{h}} \cdot \mathbf{v} d\Gamma_N \quad (11.40)$$

$$\int_{\Omega} (\nabla \cdot \mathbf{u}) \mathbf{q} d\Omega = 0 \quad (11.41)$$

The weak form for the Brinkman equation reads: Find $u \in V_g = \{u \in H^1(\Omega), u|_{\Gamma_D} = \tilde{u}\}$ and $p \in P = \{p|p \in H^1(\Omega)\}$ such that

$$\int_{\Omega} \varepsilon(-pI + 2\frac{\mu}{\varepsilon}\mathbf{D}) : \nabla \mathbf{v} \, d\Omega + \int_{\Omega} (\frac{\varepsilon\mu}{K}\mathbf{u}) \cdot \mathbf{v} \, d\Omega + \int_{\Omega} \rho(\mathbf{u} \cdot \nabla \frac{\mathbf{u}}{\varepsilon}) \cdot \mathbf{v} \, d\Omega = \int_{\Gamma_N} \varepsilon \tilde{\mathbf{h}} \cdot \mathbf{v} \, d\Gamma_N \quad (11.42)$$

$$\int_{\Omega} (\nabla \cdot \mathbf{u}) \mathbf{q} \, d\Omega = 0 \quad (11.43)$$

Finally, the weak form for Convection-Diffusion equation reads: *Find* $c \in C = \{c \in \mathbf{H}^1(\Omega)\}$ such that

$$\int_{\Omega} \frac{\partial c}{\partial t} \mathbf{v} \, d\Omega - \int_{\Omega} (\nabla \cdot (\mathbf{u}c)) \mathbf{v} \, d\Omega + \int_{\Omega} (D\nabla c) \cdot \nabla \mathbf{v} \, d\Omega = \int_{\Gamma_N} (D\nabla c \cdot \mathbf{n}) \cdot \mathbf{v} \, d\Gamma_N \quad (11.44)$$

Discretization

Approximating the variable fields with

$$\mathbf{u}(\mathbf{x}) \approx \mathbf{u}^h(\mathbf{x}) = \sum_{A=1}^{nu} N_u^A(\mathbf{x}) \mathbf{u}_A \quad (11.45)$$

$$\mathbf{u}^h(\mathbf{x}) \in \mathbf{U}^h \subset \mathbf{U} \quad (11.46)$$

where $\mathbf{U} = \{\mathbf{u} \mid \mathbf{u} \in \mathbf{H}^1, \mathbf{u} = \mathbf{u}_D \text{ in } \Gamma_D\}$.

$$p(\mathbf{x}) \approx p^h(\mathbf{x}) = \sum_{l=1}^{np} N_p^l(\mathbf{x}) p_l \quad (11.47)$$

$$p^h(\mathbf{x}) \in P^h \subset \mathbf{P} \quad (11.48)$$

where $\mathbf{P} = \{p \mid p \in \mathbf{H}^1\}$. Approximating the test functions of the velocities:

$$v(x) \approx v^h(x) = \sum_{B=1}^{nu} N_u^B(x) \delta v_B \quad (11.49)$$

$$v^h(x) \in \mathbf{V}^h \subset \mathbf{V} \quad (11.50)$$

Approximating the test functions of the pressure:

$$q(x) \approx q^h(x) = \sum_{J=1}^{nu} N_p^J(x) \delta q_J \quad (11.51)$$

$$q^h(x) \in \mathbf{Q}^h \subset \mathbf{Q} \tag{11.52}$$

The discrete form of the weak form equations can be written as algebraic equations:

$$\mathbf{K}\mathbf{u}_A + \mathbf{Q}^T \mathbf{p}_I + \mathbf{N}(\mathbf{u}_A)\mathbf{u}_A = \mathbf{F} \tag{11.53}$$

$$\mathbf{Q}\mathbf{u}_A = \mathbf{0} \tag{11.54}$$

where the convection matrix N is:

$$\mathbf{N}(\mathbf{u}_A) = \sum_{e=1}^{n_{el}} \mathbf{n}^e(\mathbf{u}_A) \tag{11.55}$$

with

$$\mathbf{n}^e = \begin{bmatrix} n(\mathbf{u}_A)^{11} \mathbf{I}_{ndim} & \cdots & n(\mathbf{u}_A)^{1n_u} \mathbf{I}_{ndim} \\ \vdots & \ddots & \vdots \\ n(\mathbf{u}_A)^{n_u 1} \mathbf{I}_{ndim} & \cdots & n(\mathbf{u}_A)^{n_u n_u} \mathbf{I}_{ndim} \end{bmatrix} \tag{11.56}$$

and the coefficients $n(\mathbf{u}_A)^{\alpha\beta}$ can be obtained as follows:

$$n(\mathbf{u}_A)^{\alpha\beta} = \rho_f \int_{\Omega_e} N_u^\alpha \mathbf{u}^h \cdot \nabla N_u^\beta d\Omega_e \quad (\alpha, \beta = 1, \dots, n_u) \tag{11.57}$$

The viscosity matrix \mathbf{K} is:

$$\mathbf{K} = \sum_{e=1}^{n_{el}} \mathbf{k}^e \tag{11.58}$$

with

$$\mathbf{k}^e = \begin{bmatrix} k^{11} \mathbf{I}_{ndim} + \mathbf{k}^{11} & \cdots & k^{1n_u} \mathbf{I}_{ndim} + \mathbf{k}^{1n_u} \\ \vdots & \ddots & \vdots \\ k^{n_u 1} \mathbf{I}_{ndim} + \mathbf{k}^{n_u 1} & \cdots & k^{n_u n_u} \mathbf{I}_{ndim} + \mathbf{k}^{n_u n_u} \end{bmatrix} \tag{11.59}$$

and the coefficients $k^{\alpha\beta}$ can be obtained by:

$$k^{\alpha\beta} = \mu \int \nabla N_u^\alpha \cdot \nabla N_u^\beta d\Omega_e \quad (\alpha, \beta = 1, \dots, n_u) \tag{11.60}$$

and the matrices $k^{\alpha\beta}$ are:

$$k^{\alpha\beta} = \begin{bmatrix} k_{11}^{\alpha\beta} & \cdots & k_{1ndim}^{\alpha\beta} \\ \vdots & \ddots & \vdots \\ k_{ndim}^{\alpha\beta} & \cdots & k_{ndim\ ndim}^{\alpha\beta} \end{bmatrix} \tag{11.61}$$

with the elements $k_{rs}^{\alpha\beta}$:

$$k_{rs}^{\alpha\beta} = \mu \int_{\Omega_e} N_{u,s}^\alpha \cdot N_{u,r}^\beta \, d\Omega \quad (\alpha, \beta = 1, \dots, n_u) \quad (r, s = 1, \dots, n_{dim}) \tag{11.62}$$

Matrix of pressure and incompressibility is:

$$\mathbf{Q} = \sum_{e=1}^{n_{el}} q^e \tag{11.63}$$

with

$$q^e = \begin{bmatrix} \varrho^{11^T} & \cdots & \varrho^{1n_u^T} \\ \vdots & \ddots & \vdots \\ \varrho^{np1^T} & \cdots & \varrho^{np\ nu^T} \end{bmatrix} \tag{11.64}$$

where the vectors $\varrho^{\gamma\beta^T}$ are:

$$\varrho^{\gamma\beta^T} = [\varrho_1^{\gamma\beta}, \dots, \varrho_{ndim}^{\gamma\beta}] \tag{11.65}$$

and

$$\varrho_r^{\gamma\beta} = - \int_{\Omega_e} N_p^\gamma N_{u,r}^\beta \, d\Omega_e \quad (\gamma = 1, \dots, n_p) \quad (\beta = 1, \dots, n_u) \quad (r = 1, \dots, n_{dim}) \tag{11.66}$$

The forcing vector F is:

$$\mathbf{F} = \sum_{e=1}^{n_{el}} f_e \tag{11.67}$$

where

$$f^e = \begin{bmatrix} \zeta^1 \\ \vdots \\ \zeta^{nu} \end{bmatrix} \tag{11.68}$$

The vectors $\zeta^{\alpha T}$ are:

$$\zeta^{\alpha T} = [\zeta_1^\alpha, \dots, \zeta_{ndim}^\alpha] \quad (11.69)$$

and

$$\zeta_r^\alpha = \int_{\Gamma_n} N_p^\alpha h_r d\Gamma_n \quad (\alpha = 1, \dots, n_p) \quad (r = 1, \dots, ndim) \quad (11.70)$$

Assumptions and Boundary Conditions

Due to the complex interactions of all the physical and chemical processes taking place, it is necessary to consider some simplifications and assumptions in order to computationally solve the problem. The model simplifications and assumptions are as follows:

1. the wall is considered rigid,
2. chemical interactions and the influence of the electric charge of the cells are neglected,
3. the cells are considered solid spheres,
4. Magnus effect are considered negligible (does not consider particle rotational effects),
5. the domains are saturated by the moving fluid, so that there are no capillarity effects,
6. and assume the model relies purely on fluid-particle interactions, so any particle-particle interaction is currently neglected.

Figure 11.1 depicts the geometry that consists of an in vitro cell culture system (hydrogel) with the objective of quantifying the major factors that affect the cell migration process at the macro-scale. This three-dimensional geometry emulates a simplified vascularized tumor system with the hydrogel acting as the tumor tissue and a microchannel acting as a vessel. This simple system was chosen for conducting the simulations because it will be easily developed during experimental tests in future work. The hydrogel was considered as a homogeneous porous media for this case. The objective of this study case is to understand the pressure effects, distribution of nutrients, drag interactions, and viscous shear stress exertions on cell motion at the macro-scale. A finite element method was implemented to solve the mathematical model. Tetrahedral elements were used to mesh the three-dimensional computational domain and mesh sensitivity analysis was carried out by varying the number of mesh elements in the domain.

The boundary conditions specify that there is no slip at the wall, upstream flow varies in a parabolic fashion, and there is free flow at the outlet. The tube is long enough to generate developed axial velocity profiles.

The parameters used in the simulation, in Table 11.1, consist of both estimated and experimental values. The velocity inlet was 5.45 mm/s, which was calculated based on the volume flow rate of $Q = 0.130$ mL/min.

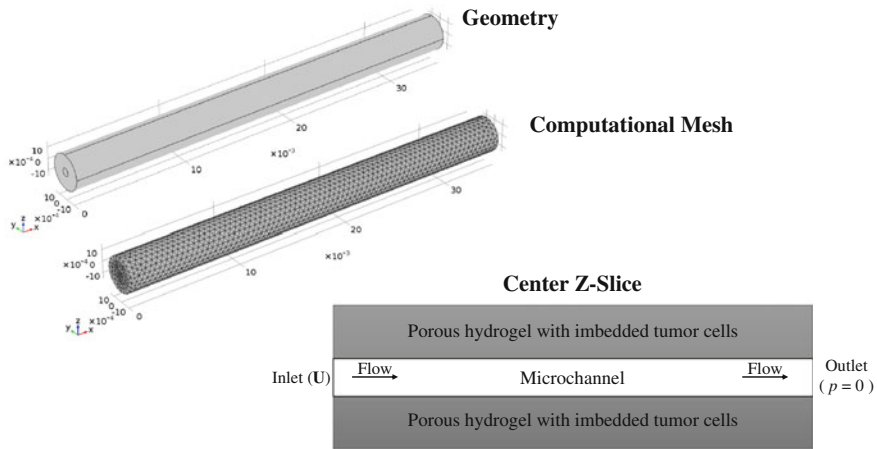


Fig. 11.1 Geometry of the hydrogel at the macro-scale

Table 11.1 Macro-scale simulation parameters

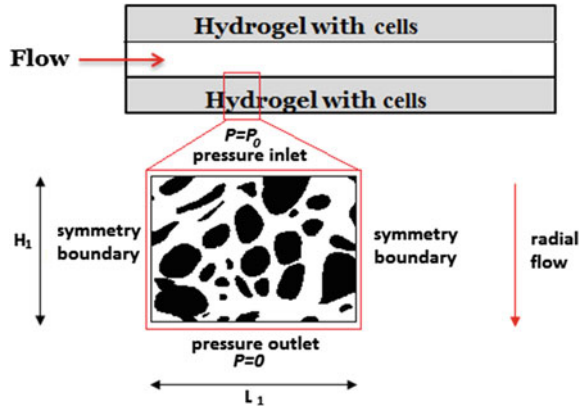
Parameter	Value (hydrogel)	Value (microchannel)
Nutrient attraction (M) [$J\ m^3/mol$]	5×10^{-4}	5×10^{-4}
Force from hydrogel (K) [$N\ s/m$]	1×10^{-4}	1×10^{-4}
Dynamic viscosity (μ) [$Pa\ s$]	1.3	7.8×10^{-4}
Permeability (k) [m^2]	1	1
Porosity (ϵ)	0.9	1
Density (ρ) [kg/m^3]	3,000	1,000

Nanoparticles can be used to passively target tumor tissue through leaky blood vessels. Nanoparticles with less than 200 nm diameters easily pass through these leaky vessel walls; thus they are capable of targeting tumors [28]. This simulation, therefore, includes nanoparticles that are smaller than 200 nm. Although the hydrogel has a three-dimensional porous structure, this first approach was simplified in 2D as shown in Fig 11.2.

11.3.1.2 Macro-scale Results

Although the flow in the human circulatory system is unsteady in response to pulsatile pressure, steady flow models, like the model introduced in this section, provide useful information about the aspects of fluid flow. This case was considered steady flow. A parabolic fluid flow was introduced at the inlet and nutrients were introduced into the same inlet as fluid flow into the microchannel and hydrogel. Particles imbedded in the hydrogel migrated in response to their attraction to the nutrients.

Fig. 11.2 Network of the hydrogel



The simulation results of Fig. 11.3 describe the movement of the cells due to advection and diffusion at macro-scale and only displays cells that have a velocity greater than 0.1 mm/s. Advection involves the movement of the cells through the microchannel and hydrogel at the rate of movement of the fluid carrier. Diffusion is caused by the motion of the cells from zones of high concentration to zones of lower concentration. The accuracy of the simulation results was improved by employing a finer mesh that contains one cell per element.

11.3.1.3 Micro-scale Results

The velocity magnitude is higher in the narrowest pores and tends to decrease where the pore channel size increases. However, there is a considerable zone with low flow velocity levels where the permeability would be affected possibly by the increase of the pore path (tortuosity). This may imply that this area would be susceptible to cell attachment and deposition.

Simulation cases with differing pressure gradients at steady state were conducted with the results indicating that the distribution of the velocities, pressure, and shear stress were similar for three cases inside the wall of the hydrogel. Different Reynolds numbers and shear stresses, in Table 11.2, were obtained in the three cases.

Figure 11.4 displays the transport phenomena related to advection and diffusion inside the hydrogel, the mechanical dispersion, and the mixing of the cells due to changes in fluid velocities along the streamlines. These variations are associated with three phenomena: pore size, pore friction, and path length. Figure 11.4a depicts how some particles gain inertia in the narrowest pores. Figure 11.4b shows stagnant zones where some cells might interact with other cells and the wall.

Figure 11.4c shows deposition points close enough to the wall, where the cells might be attracted due to the weak forces known as van der Waal's (assuming absence of electrical charge of the cells) [29]. The trapped particles might act like an extension

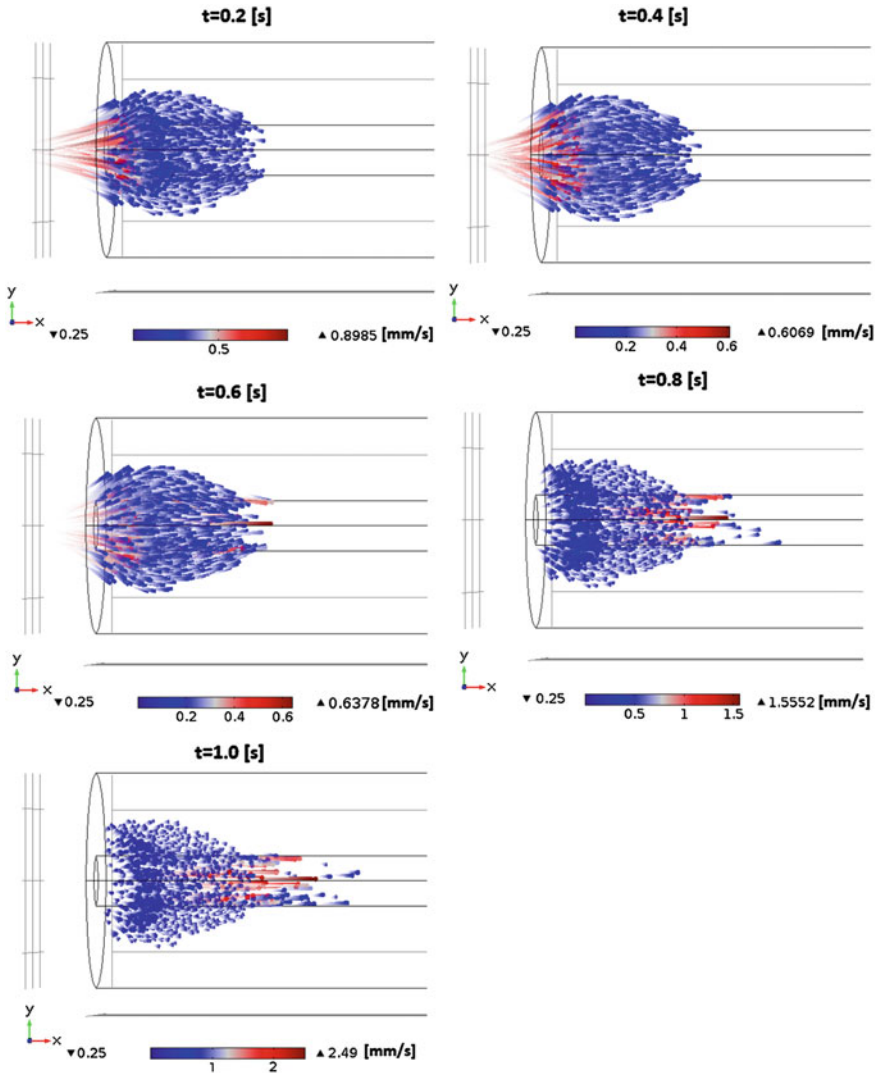


Fig. 11.3 Time evolution of cell transport (only cells with velocity greater than 0.1 mm/s)

of the wall and trap other particles or block pores at various sites. The fast moving particles with higher inertia may not become trapped. Figure 11.4d and e shows zones of bad irrigation of nutrients and recirculation, where the lack of nutrients might affect the cells viability and consequently promote mechanical stimulus into biochemical reactions near to the wall (mechanotransduction).

Table 11.2 Reynolds average and maximum values of shear stress considering a blood density at 37 °C = 1,060 [kg/m³] and blood dynamic viscosity = 0.005 [Pa s]

Pressure gradient [Pa]	Reynolds average	Max Shear stress [dynes/cm ²]
0.10	1.21	0.23
1.00	9.32	1.99
10.0	57.9	12.4

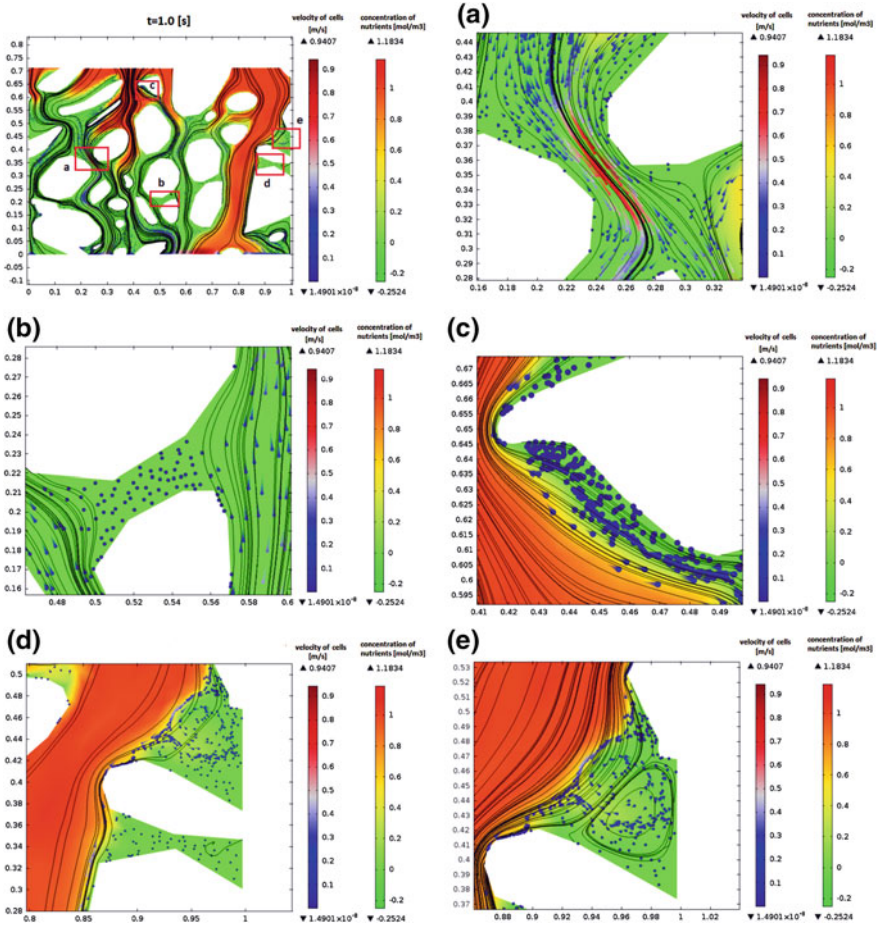


Fig. 11.4 Different phenomena of dispersion over the particles inside the wall: **a** effect of a narrow pore channel; **b** stagnation points; **c** deposition; **d** bad irrigation; **e** recirculation zones

11.3.2 Bone Remodeling and Wound Healing

In general, mixture theory provides a comprehensive framework [30] that allows multiple species to be included under the abstract notion of a continuous media. In this framework, biological tissue can be considered as a multi-phasic system with different species, including solid tissue, body fluids, cells, extracellular matrix (ECM), nutrients, etc. The species (or constituents) are denoted by ϕ_α ($\alpha = 1, 2, \dots, \kappa$), where κ is the number of species in the mixture. The nominal densities of each constituent is denoted by ρ^α and the true densities are denoted by $\rho^{\alpha R}$.

To introduce a formal characterization of the volume fraction, a domain occupying the control space B_S is defined with the boundary ∂B_S , in which all the constituents ϕ_α occupy the volume fractions η_α , which satisfy the constraint

$$\sum_{\alpha=1}^{\kappa} \eta^\alpha(\mathbf{x}, t) = \sum_{\alpha=1}^{\kappa} \frac{\rho^\alpha}{\rho^{\alpha R}} = 1, \quad (11.71)$$

where \mathbf{x} is the position vector of the actual placement and t denotes the time.

Two frames of reference are used to describe the governing principles of continuum mechanics. The Lagrangian frame of reference is often used in solid mechanics, while the Eulerian frame of reference is used in fluid mechanics. The Lagrangian description is usually suitable to establish mathematical models for stress-induced growth, such as bone remodeling and wound healing (e.g., [31]), while the Eulerian description is often used for developing mass transfer driven tumor growth models [32–35] with a few exceptions when tumors undergo large deformations [36].

To develop mathematical models for each application, the governing equations are provided by the conservation laws, and the constitutive relations are usually developed through empirical relationships subject to constraints such as frame invariance condition and consistency with thermodynamics, to name a few. Specifically, the governing equations can be obtained from conservations of mass, momentum, and energy for each species as well as the mixture. When the free energy of the system is given as a function of dependent field variables, such as strain and temperature, the second law of thermodynamics (the Clausius-Duhem inequality) provides a means for determining forms of some constitutive equations via the well-known method of Coleman and Noll [37].

Predictive medicine is emerging as a research field as well as a potential medical tool for designing optimal treatment options by advancing deeper understanding of biological and biomedical processes and providing patient-specific prognosis and therapies. Characterizing a biological system involves studies of complex phenomena at various spatial and temporal scales. At a macro-level, continuum mechanics can be employed to investigate tissue behavior. In particular, both mixture theory and porous media theory can be used to model both hard and soft tissues in terms of growth, particle flow, bioheat transfer, etc. Mixture theory can be introduced for modeling both hard and soft tissues.

In continuum mixture theory, an arbitrary point in a continuous medium can be occupied simultaneously by many different constituents differentiated only through their volume fractions. The advantage of this mathematical representation of tissues is that it permits direct reconstruction of patient-specific geometry from medical imaging; inclusion of species from different scales as long as they can be characterized by either density or volume fraction functions; and automatically provides for interactions among species included in the mixture without the need of front tracking or complex interaction condition. Furthermore, the mathematical models based on the notion of mixture can be derived from the first principles (conservation laws and the second law of thermodynamics).

The applications considered here include bone remodeling, wound healing, and tumor growth. Models of the cardiovascular system can also be included within the mixture framework if soft tissues such as heart and vessels are treated as separate species different than fluid (blood) and the extracellular matrix.

Bone remodeling is a natural biological process that occurs during the course of maturity or after injuries, which can be characterized by a reconfiguration of the density of bone tissue due to mechanical forces or other biological stimuli. Wound healing (or cicatrization), on the other hand, mainly involves skin or other soft organ tissues that repair themselves after the protective layer and/or tissues are broken and damaged. In particular, wound healing in fasciated muscle occurs due to the presence of traction forces that accelerate the healing process. Both bone remodeling and wound healing can be investigated under the general framework of continuum mixture theory at the tissue level. Another important application is tumor growth modeling, which is relevant to cancer biology, treatment planning, and outcome prediction. The mixture theory framework can provide a convenient vehicle to simulate growth (or shrinking) phenomena under various biological conditions.

Considering the conservation of mass for each species ϕ^α in a control volume, the mass production and fluxes across the boundary of the control volume are required to be equal:

$$\frac{\partial \rho^\alpha}{\partial t} + \nabla \cdot (\rho^\alpha \mathbf{v}) = \hat{\rho}^\alpha. \quad (11.72)$$

In Eq. (11.72), the velocity of the constituent is denoted by \mathbf{v} and the mass supplies between the phases are denoted by $\hat{\rho}^\alpha$. From a mechanical point of view, the processes of bone remodeling and wound healing are mainly induced by traction forces. For simplicity, we choose a triphasic system comprised of solid, liquid, and nutrients to illustrate the modeling process [31]. The mass exchange terms are subject to the constraint

$$\sum_{\alpha=1}^{\kappa} \hat{\rho}^\alpha = 0 \quad \text{or} \quad \hat{\rho}^S + \hat{\rho}^N + \hat{\rho}^L = 0. \quad (11.73)$$

Moreover, if the liquid phase is not involved in the mass transition, then,

$$\hat{\rho}^S = -\hat{\rho}^N \quad \text{and} \quad \hat{\rho}^L = 0. \quad (11.74)$$

Next, the momentum of the constituent ϕ_α is defined by

$$\mathbf{m}^\alpha = \int_{B_\alpha} \rho^\alpha \mathbf{v}_\alpha dv. \quad (11.75)$$

By including \mathbf{m}^α in the total change of linear momentum in B_α and denoting the interaction of the momentum of the constituents ϕ_α by $\hat{\mathbf{p}}^\alpha$, the standard momentum equation (Cauchy equation of motion) for each constituent becomes

$$\nabla \cdot \mathbf{T}^\alpha + \rho^\alpha (\mathbf{b} - \mathbf{a}_\alpha) + \hat{\mathbf{p}}^\alpha - \hat{\rho}^\alpha \mathbf{v}_\alpha = \mathbf{0}, \quad (11.76)$$

where the expression $\hat{\rho}^\alpha \mathbf{v}_\alpha$ represents the exchange of linear momentum through the density supply $\hat{\rho}^\alpha$. The term \mathbf{T}^α denotes the partial Cauchy stress tensor, $\rho^\alpha \mathbf{b}$ specifies the volume force. In addition, the terms $\hat{\mathbf{p}}^\alpha$, where $\alpha = S, L, N$, are required to satisfy the constraint condition

$$\hat{\mathbf{p}}^S + \hat{\mathbf{p}}^L + \hat{\mathbf{p}}^N = \mathbf{0}. \quad (11.77)$$

In the case of either bone remodeling or wound healing, the velocity field is nearly in steady state. Thus, the acceleration can be neglected by setting $\mathbf{a}_\alpha = \mathbf{0}$. The resulting system of equations can then be written

$$\nabla \cdot \mathbf{T}^\alpha + \rho^\alpha \mathbf{b} + \hat{\mathbf{p}}^\alpha = \hat{\rho}^\alpha \mathbf{v}_\alpha. \quad (11.78)$$

The second law of thermodynamics (entropy inequality) provides expressions for the stresses in the solid and fluid phases that are dependent on the displacements and the seepage velocity, respectively. The seepage velocity is a relative velocity between the liquid and solid phases, which are often obtained from explicit Darcy velocity expressions for flow through a porous medium (solid phase). Various types of material behavior can be described in terms of principal invariants of the structural tensor \mathbf{M} and the right Cauchy-Green Tensor \mathbf{C}_S , where

$$\mathbf{M} = \mathbf{A} \otimes \mathbf{A} \quad \text{and} \quad \mathbf{C}_S = \mathbf{F}_S^T \mathbf{F}_S, \quad (11.79)$$

and \mathbf{A} is the preferred direction inside the material and \mathbf{F}_S is the deformation gradient for a solid undergoing finite deformations. The expressions for the stress in the solid are dependent on the deformation gradient and consequently the displacements of the solid. Summation of the momentum conservation equations provides the equation for the solid displacements. Mass conservation equations, with incorporation of the saturation condition, provide the equation for interstitial pressure. In addition, the mass conservation equations for each species provide the equations for the evolution of volume fractions.

Assuming the fluid phase (F) is comprised of the liquid (L) and the nutrient phases (N) we obtain ($F = L + N$)

$$\nabla \cdot \sum_{\alpha}^{S,L,N} \mathbf{T}^{\alpha} + \mathbf{b} \sum_{\alpha}^{S,L,N} \rho^{\alpha} + \sum_{\alpha}^{S,L,N} \hat{\mathbf{p}}^{\alpha} - \hat{\rho}^S \mathbf{v}_S - \hat{\rho}^F \mathbf{v}_F = 0. \quad (11.80)$$

Since $\hat{\rho}^F = -\hat{\rho}^S$, and $\hat{\mathbf{p}}^S + \hat{\mathbf{p}}^N + \hat{\mathbf{p}}^F = 0$, we obtain

$$\nabla \cdot \sum_{\alpha}^{S,L,N} \mathbf{T}^{\alpha} + \mathbf{b} \sum_{\alpha}^{S,L,N} \rho^{\alpha} + \hat{\rho}^S (\mathbf{v}_F - \mathbf{v}_S) = 0. \quad (11.81)$$

The definition of the seepage velocity \mathbf{w}_{FS} provides the following equation

$$\nabla \cdot \sum_{\alpha}^{S,F} \mathbf{T}^{\alpha} + \mathbf{b} \sum_{\alpha}^{S,F} \rho^{\alpha} + \hat{\rho}^S (\mathbf{w}_{FS}) = 0. \quad (11.82)$$

The strong form for the pressure equation can be written as follows

$$\nabla \cdot \left(\eta^F \mathbf{w}_{FS} \right) + \mathbf{I} : \mathbf{D}_S - \hat{\rho}^S \left(\frac{1}{\rho^{SR}} - \frac{1}{\rho^{NR}} \right) = 0. \quad (11.83)$$

The strong form of mass conservation equation for the solid phase is

$$\frac{D^S(\eta^S)}{Dt} + \eta^S \mathbf{I} : \mathbf{D}_S = \frac{\hat{\rho}^S}{\rho^{SR}}. \quad (11.84)$$

Finally, the balance of mass for the nutrient phase can be described as

$$\frac{D^S(\eta^N)}{Dt} - \frac{\hat{\rho}^N}{\rho^{NR}} + \eta^N \mathbf{I} : \mathbf{D}_S + \nabla \cdot \left(\eta^N \mathbf{w}_{FS} \right) = 0. \quad (11.85)$$

In the above, \mathbf{w}_{FS} is the seepage velocity, \mathbf{D}_S denotes the symmetric part of the spatial velocity gradient, and $\frac{D^S(\cdot)}{Dt}$ denotes the total derivative of quantities with respect to the solid phase. The seepage velocity is obtained from

$$\mathbf{w}_{FS} = \frac{1}{\mathbf{S}_F} \left[\lambda \nabla \eta^F - \hat{\mathbf{p}}^F \right], \quad (11.86)$$

Here, \mathbf{S}_F is the permeability tensor, λ denotes the pressure, and η^F is the volume fraction of the fluid. Equations 11.78–11.85 are required to be solved for the bone remodeling problem with the mixture theory. The primary dependent variables are $\{\mathbf{u}_S, \lambda, n_S, n_N\}$, the solid displacements, interstitial pressure, and the solid and nutrient volume fractions.

Bone remodeling is an important biological application that can be studied within the aegis of the above mathematical framework. The process of bone remodeling involves three types of cells namely osteoblasts, osteocytes, and osteoclasts. The remodeling process is a continuous process and annually around 10 % of the bone is replaced. It is driven by the requirement of calcium in the extracellular fluid, and can also occur in response to mechanical stresses on the bone tissue. The above framework presented studies the bone reconfiguration due to external stress. One example of bone remodeling is a femur under traction loadings, which drives the process so that the bone density is redistributed. Based on the stress distribution, the bone usually becomes stiffer in the areas of higher stresses.

The same set of equations can also be used to study the process of wound healing. It is obvious, however, that the initial and boundary conditions are specified differently. It is worth noting that traction forces inside the wound can facilitate the closure of the wound. From the computational point of view, the specification of solid and liquid volume fractions as well as pressure are required on all interior and exterior boundaries of the computational domain. The interior boundary is assumed to be inside surface exposed due to the wounding of the tissue.

The interior boundary (inner face) of the wound can be assumed to possess a sufficiently large quantity of the solid and liquid volume fractions, which is modeled biologically with sufficient nutrient supply at this face. On the other hand, the opening of the wound can be prescribed with natural boundary conditions with seepage velocity.

11.3.3 Modeling Tumor Growth

Attempts at developing computational mechanics models of tumor growth date back over half a century (see, e.g., [38]). Various models have been proposed based on ordinary differential equations (ODE) e.g., ([39–42]), extensions of ODE's to partial differential equations [33, 43] or continuum mechanics based descriptions that study both vascular and avascular tumor growth. Continuum mechanics-based formulations consider either a Lagrangian [31] or an Eulerian description of the medium [33]. Various considerations such as modifications of the ordinary differential equations (ODE's) to include effects of therapies [41], studying cell concentrations in capillaries during vascularization with and without inhibitors, multiscale modeling [2, 4, 44–46], and cell transport equations in the extracellular matrix (ECM) [34] have been included.

Modeling tumor growth can also be formulated under the framework of mixture theory with a multi-constituent description of the medium. It is convenient to use an Eulerian frame of reference. Other descriptions have considered the tumor phase with diffused interface [35]. Consider, the volume fraction of cells denoted by (ξ) , extracellular liquid (l) , and extracellular matrix (m) [33]. The governing equations are derived from conservation laws for each constituent of the individual phases.

The cells can be further classified as tumor cells, epithelial cells, fibroblasts, etc. denoted by subscript, $\alpha = 1, 2, \dots, N$. Similarly, we can distinguish different components of the extra-cellular matrix (ECM) namely, collagen, elastin, fibronectin, vitronectin, etc. [47] denoted by subscript $\beta = 1, 2, \dots, M$. The ECM component velocities are assumed to be the same, based on the constrained submixture assumption [34]. The concentrations of chemicals within the liquid are of interest in the extracellular liquid. The above assumptions lead to the mass conservation equations for the constituents as (ξ , m , and l),

$$\begin{aligned} \frac{\partial \xi_\alpha}{\partial t} + \nabla \cdot (\xi_\alpha v_{\xi_\alpha}) &= \Gamma_{\xi_\alpha}, \\ \frac{\partial m_\beta}{\partial t} + \nabla \cdot (m_\beta v_m) &= \Gamma_{m_\beta}. \end{aligned} \quad (11.87)$$

In the equations above v_{ξ_α} and v_m denote the velocities of the respective phases. Note that no subscript on v_m (constrained submixture assumption). Mass balance equation expressed as concentrations in the liquid phase are expressed as

$$\frac{\partial c}{\partial t} = \nabla \cdot (D \nabla c) + G. \quad (11.88)$$

Here, D denotes the effective diffusivity tensor in the mixture, G contains the production/source terms and degradation/uptake terms relative to the entire mixture. The system of equations requires the velocities of each component to obtain the closure. The motion of the volume fraction of the cells are governed by the momentum equations

$$\rho \xi \left(\frac{\partial v_\xi}{\partial t} + v_\xi \cdot \nabla v_\xi \right) = \nabla \cdot \tilde{T}_\xi + \rho \xi \mathbf{b} + \tilde{m}_\xi. \quad (11.89)$$

Similar expressions hold for the extracellular matrix and the liquid phases. The presence of the saturation constraint requires one to introduce a Lagrange multiplier into the Claius-Durhem inequality and provides expressions for the excess stress \tilde{T}_ξ and excess interaction force m_ξ . The Lagrange multiplier is classically identified with the interstitial pressure P . Body forces, \mathbf{b} are ignored for the equations for the ECM and the excess stress tensor in the extracellular liquid is assumed to be negligible in accordance with the low viscous forces in porous media flow studies. With these assumptions, we obtain the following equations

$$\begin{aligned} -\xi_\alpha \nabla P + \nabla \cdot (\xi_\alpha T_{\xi_\alpha}) + m_{\xi_\alpha} + \rho \xi_\alpha b_\alpha &= 0, \\ -m \nabla P + \nabla \cdot (m T_m) + m_m &= 0, \\ -l \nabla P + m_l &= 0. \end{aligned} \quad (11.90)$$

These equations provide the governing differential equations required to solve tumor growth problems. The primary variables to be solved are $\{\xi_\alpha, m_\beta, P\}$.

The governing equations can be solved with suitable boundary conditions of specified volume fractions of the cells, extracellular liquid, and pressures. Fluxes of these variables across the boundaries also need to be specified for a complete description of the problem.

Other approaches in modeling tumor growth involve tracking the moving interface of the growing tumor. Among them is the phase field approach. The derivation of the basic governing equations is given in Wise [32]. From the continuum advection-reaction-diffusion equations, the volume fractions of the tissue components obey

$$\frac{\partial \phi}{\partial t} + \nabla \cdot (\mathbf{u}\phi) = -\nabla \cdot \mathbf{J} + S. \quad (11.91)$$

Here, ϕ denotes the volume fraction, \mathbf{J} denotes the fluxes that account for the mechanical interactions among the different species, and the source term S accounts for the inter-component mass exchange as well as gains due to proliferation and loss due to cell death.

The above Eq. (11.91) is interpreted as the evolution equation for ϕ which characterizes the phase of the system. This approach modifies the equation for the interface to provide both for convection of the interface along with an appropriate diminishing of the total energy of the system. The free energy of a system of two immiscible fluids consists of mixing, bulk distortion, and anchoring energy. For simple two-phase flows, only mixing energy is retained, which results in a rather simple expression for the free energy ϕ

$$F(\phi, \nabla\phi, T) = \int \left(\frac{1}{2} \epsilon^2 |\nabla\phi|^2 + f(\phi, T) \right) dV = \int f_{\text{tot}} dV. \quad (11.92)$$

Physical processes involve those in which the total energy is minimized. The following equation describes evolution of the phase field parameter:

$$\frac{\partial \phi}{\partial t} + \mathbf{u}\nabla\phi = \nabla \cdot \gamma \nabla \left(\frac{\partial f_{\text{tot}}}{\partial \phi} - \nabla \cdot \frac{\partial f_{\text{tot}}}{\partial \nabla\phi} \right) \quad (11.93)$$

where, f_{tot} is the total free energy of the system. Equation (11.93) seeks to minimize the total free energy of the system with a relaxation time controlled by the mobility γ . With some further approximations, the partial differential equation governing the phase field variable is obtained as the Cahn-Hilliard equation,

$$\frac{\partial \phi}{\partial t} + \mathbf{u}\nabla\phi = \nabla \cdot \gamma \nabla G, \quad (11.94)$$

where G is the chemical potential. The mobility (γ) determines the timescale of the Cahn-Hilliard diffusion and must be large enough to retain a constant interfacial thickness but small enough so that the convective terms are not overly damped.

The mobility is defined as a function of the interface thickness as $\gamma = \chi\epsilon^2$. The chemical potential is provided by

$$G = \lambda \left[-\nabla^2 \phi + \frac{\phi(\phi^2 - 1)}{\epsilon^2} \right]. \quad (11.95)$$

The Cahn-Hilliard equation forces ϕ to take values of -1 or $+1$ except in a very thin region on the fluid-fluid interface. The above equation is of fourth order and poses a formidable challenge to solve. The solutions are characterized by nearly constant states, with complex morphologies, separated by evolving narrow transition layers that describe diffuse interfaces between tumor and host tissues.

The presence of the fourth-order term poses stringent restrictions on the time step. The step size for time integration of the above equation is constrained by h^4 where h is the spatial grid size. To remove this restriction one can use a Crank-Nicholson-like time integration method, which results in non-linear equations at the implicit time level. Multilevel nonlinear *full approximation storage* (FAS) multi-grid method is adopted to solve the discrete system, with respect to time and space. When taking the finite difference approach for the spatial discretization of the Cahn-Hilliard equation one starts with a central difference approximation of the derivative in space along with a backward difference approximation of the time derivative. Alternatively, Crank-Nicholson approximation scheme can be implemented for time discretization, with an appropriate treatment of the advection term. Higher order approximation of the divergence and the gradient operators are obtained from the appropriate Taylor series terms in constructing the discrete forms. The advection terms need special treatment to avoid numerical oscillations at the tumor-host interface.

In the finite difference framework various schemes have been proposed to discretize the advective flux. In specific for the phase field approach the advection operator appears as a shock term which needs to be stabilized. Classical discretization methods, such as the central difference approximation, have the disadvantage of causing non-physical oscillations across or in the near vicinity of discontinuities known as the Gibbs phenomenon. To suppress the Gibbs phenomenon, Harten [48] proposed an essentially non-oscillatory scheme (ENO) scheme based on the Godunov upwind scheme, which achieves an accuracy of arbitrary high order. Efforts toward improving the ENO scheme have resulted in the development of weighted non-oscillatory scheme or the WENO scheme [49].

Finite element analysis of Cahn-Hilliard equation have also been accomplished [50–52]. Error bounds of the Cahn-Hilliard equation with degenerate mobility were examined in Barrett [50]. Both convergence and well-posed finite element approximation were examined in addition to determining the stability bounds of the approximation. The existence of the Lyapunov energy functional was found to be of primary importance in the error analysis [51]. Backward difference in time was utilized and optimal error bounds were established. Usage of multi-grid methods for solving Cahn-Hilliard equation without the presence of the advection term have been presented in Kay [52]. Implicit backward Euler stepping in time in conjugation with continuous piecewise linear basis functions in space were found to provide

faithful results. Conservation of the total energy of the Lyapunov energy functional provided further confirmation of the accuracy of the simulation. A multi-grid scheme was proposed to solve the problem in opposition to Gauss-Seidel variants as solvers for the discrete system.

The introduction of the phase field interface allows the fourth-order Cahn-Hilliard equation to be written as a set of two second order PDEs

$$\frac{\partial \phi}{\partial t} + \mathbf{u} \cdot \nabla \phi = \nabla \cdot \frac{\gamma \lambda}{\epsilon^2} \nabla \psi, \quad (11.96)$$

$$\psi = -\nabla \cdot \epsilon^2 \nabla \phi + (\phi^2 - 1)\phi. \quad (11.97)$$

The above equation is the simplest phase field model, and is known as model A in the terminology of phase field transitions [4, 35, 53]. Phase field approaches have been applied for solving the tumor growth and multiphase descriptions of an evolving tumor have been obtained with each phase having its own interface and a characteristic front of the moving interface obtained with suitable approximations.

When specific applications of the phase field approach to tumor growth are considered, the proliferative and non-proliferative cells are described by the phase field parameter ϕ . The relevant equations in the context of tumor growth are provided by the following [35, 54]

$$\frac{\partial \phi}{\partial t} = M \nabla^2 \left[-\phi + \phi^3 - \epsilon \nabla^2 \phi \right] + \alpha_p(T) \phi \Theta(\phi). \quad (11.98)$$

Here, M denotes the mobility coefficient, T stands for the concentration of hypoxic cell produced angiogenic factor, and $\Theta(\phi)$ denotes the Heaviside function which takes a value of 1 when its argument is positive. The proliferation rate is denoted by $\alpha_p(T)$ and as usual ϵ denotes the width of the capillary wall. The above equation is solved with the governing equation for the angiogenic factor T . The angiogenic factor diffuses randomly from the hypoxic tumor area where it is produced and obeys the following equation

$$\frac{\partial T_i}{\partial t} = \nabla \cdot (D \nabla T) - \alpha_T T \phi \Theta(\phi). \quad (11.99)$$

In the equation above D denotes the diffusion coefficient of the factor in the tissue and α_T denotes the rate of consumption by the endothelial cells.

11.4 Open Questions

Multiscale methods have been used in a wide range of applications: materials and nanomaterials science [55, 56], elasticity and plasticity analysis [57], computational biomechanics [58], drug development [59], vascular tumor growth [44], coarse-grain

peptide and protein folding modeling [60–62], mutation and immune competition of cancer cells [63], organ level analysis [64], computational physiology [65], and genetic regulatory networks [66]. The common goal of all these applications is to create a predictive multiscale mathematical model to simulate a complex system.

The open question that spans each application of multiscale modeling is how to validate and calibrate the model with experimental data. Although still a useful tool, a mathematical model does not become a predictive tool until it has been validated and calibrated with experimental data [56]. Another limitation and open question of current multiscale methods is how to easily extend the analysis to three dimensions. Most of the methods described in this chapter are useful only in one or two dimensions [1]. Currently available multiscale methods have tremendous challenge in dealing with nonlinear problems [67].

Moreover, a consistent difficulty in multiscale mathematical modeling is how to bridge spatial and temporal scales in a systematic and seamless fashion. In many biological phenomena, such as protein folding and cell proliferation, events at small scales occur much quicker than events at larger scales. In some cases, multiscale methods provide the tools to handle the different spatial scales, but not the temporal scales [1, 5, 6, 8, 10–12, 14, 15].

The future direction of multiscale modeling calls for developing mathematical methods to apply in three dimensions with the ability to simultaneously bridge spatial and temporal scales. These additional capabilities will allow for development of more biologically relevant and useful predictive models.

Acknowledgments The authors would like to express our sincere gratitude to J. Cliff Zhou for his early involvement in this work, and Dr. M.N. Rylander and her group for providing information regarding the 3D in vitro cell culture system. The funding from NSF/CREST program #0932339 is highly appreciated and acknowledged.

References

1. W.K. Liu, E.G. Karpov, H.S. Park, *Nano mechanics and materials: theory, multiscale methods and applications* (Wiley, 2006).
2. T.S. Deisboeck, G.S. Stamatakis, *Multiscale cancer modeling*, vol. 34 (CRC Press LLC, 2010).
3. S. Schnell, R. Grima, P. Maini, *Am. Sci.* 95(2), 134 (2007).
4. V. Cristini, J. Lowengrub, *Multiscale modeling of cancer: an integrated experimental and mathematical modeling approach* (Cambridge University Press, 2010).
5. S. Xiao, T. Belytschko, *Computer methods in applied mechanics and engineering* 193(17), 1645 (2004).
6. S. Zhang, R. Khare, Q. Lu, T. Belytschko, *International Journal for Numerical Methods in Engineering* 70(8), 913 (2007).
7. R. Sunyk, P. Steinmann, *International Journal of Solids and Structures* 40(24), 6877 (2003).
8. E.B. Tadmor, M. Ortiz, R. Phillips, *Philosophical Magazine A* 73(6), 1529 (1996).
9. J. Oden, T. Strouboulis, P. Devloo, *Computer Methods in Applied Mechanics and Engineering* 59(3), 327 (1986).
10. W.A. Curtin, R.E. Miller, *Modelling and simulation in materials science and engineering* 11(3), R33 (2003).

11. L. Shilkrot, R. Miller, W. Curtin, *Physical review letters* 89(2), 025501 (2002).
12. L. Shilkrot, R.E. Miller, W.A. Curtin, *Journal of the Mechanics and Physics of Solids* 52(4), 755 (2004).
13. E. Van der Giessen, A. Needleman, *Modelling and Simulation in Materials Science and Engineering* 3(5), 689 (1995).
14. F.F. Abraham, J.Q. Broughton, N. Bernstein, E. Kaxiras, *EPL (Europhysics Letters)* 44(6), 783 (1998).
15. R.E. Rudd, J.Q. Broughton, *Physical Review B* 58(10), R5893 (1998).
16. N.V. Mantzaris, S. Webb, H.G. Othmer, *Journal of mathematical biology* 49(2), 111 (2004).
17. M.A. Chaplain, S.R. McDougall, A. Anderson, *Annu. Rev. Biomed. Eng.* 8, 233 (2006).
18. A.R. Anderson, *Mathematical Medicine and Biology* 22(2), 163 (2005).
19. J. Berthier, P. Silberzan, *Microfluidics for biotechnology*. Second Edition. (Artech House, 2010).
20. B.M. OConnell, M.T. Walsh, *Annals of biomedical Engineering* 38(4), 1354 (2010).
21. K. Vafai, *Porous media: Application in biological systems and biotechnology* (CRC Press, 2011).
22. B. Verleye, M. Klitz, R. Croce, D. Roose, S. Lomov, I. Verpoest, *Computation of the Permeability of Textiles (SFB 611, 2006)*.
23. C.C. Wong, *Modelling the effects of textile preform architecture on permeability*. Ph.D. thesis, The University of Nottingham (2006).
24. A.F.S. Rahul Vallabh, Pamela Banks-Lee, *Journal of Engineered Fibers and Fabrics* 5(3), 7 (2010).
25. K.B. Chandran, A.P. Yoganathan, S.E. Rittgers, *Biofluid mechanics: the human circulation* (CRC Press, 2012).
26. M.H. Kroll, *The Journal of The American Society of Hematology* 88, No. 5 (September 1), 1525 (1996).
27. R.L. Fournier, *Basic Transport Phenoma in Biomedical Engineering* (Taylor and Francis Group, 2007).
28. K. Lee, H. Lee, K.H. Bae, T.G. Park, *Biomaterials* 31(25), 6530 (2010).
29. K. Sutherland, *Filters and filtration Handbook* (Elsevier, 2008).
30. R. Atkin, R. Craine, *The Quarterly Journal of Mechanics and Applied Mathematics* 29(2), 209 (1976).
31. T. Ricken, A. Schwarz, J. Bluhm, *Computational materials science* 39(1), 124 (2007).
32. S. Wise, J. Lowengrub, H. Frieboes, V. Cristini, *Journal of theoretical biology* 253(3), 524 (2008).
33. D. Ambrosi, L. Preziosi, *Mathematical Models and Methods in Applied Sciences* 12(05), 737 (2002).
34. L. Preziosi. *Cancer modeling and simulation. mathematical and computational biology* (2003).
35. J.T. Oden, A. Hawkins, S. Prudhomme, *Mathematical Models and Methods in Applied Sciences* 20(03), 477 (2010).
36. D. Ambrosi, F. Mollica, *International Journal of Engineering Science* 40(12), 1297 (2002).
37. B.D. Coleman, W. Noll, *Archive for Rational Mechanics and Analysis* 13(1), 167 (1963).
38. P. Armitage, R. Doll, *British journal of cancer* 8(1), 1 (1954).
39. J.P. Ward, J. King, *Mathematical Medicine and Biology* 14(1), 39 (1997).
40. D. Grecu, A. Carstea, A. Grecu, A. Visinescu, *Romanian Reports in Physics* 59(2), 447 (2007).
41. J.P. Tian, K. Stone, T.J. Wallin, *DYNAMICAL SYSTEMS* pp. 771–779 (2009).
42. B.A. Lloyd, D. Szczerba, G. Székely, in *Medical Image Computing and Computer-Assisted Intervention-MICCAI 2007* (Springer, 2007), pp. 874–881.
43. T. Roose, S.J. Chapman, P.K. Maini, *Siam Review* 49(2), 179 (2007).
44. P. Macklin, S. McDougall, A.R. Anderson, M.A. Chaplain, V. Cristini, J. Lowengrub, *Journal of mathematical biology* 58(4–5), 765 (2009).
45. W.Y. Tan, *Handbook of cancer models with applications*, vol. 9 (World Scientific, 2008).
46. D. Wodarz, N.L. Komarova, *Computational biology of cancer: lecture notes and mathematical modeling* (World Scientific Publishing Company, 2005).

47. S. Astanin, L. Preziosi, in *Selected Topics in Cancer Modeling* (Springer, 2008), pp. 1–31.
48. A. Harten, B. Engquist, S. Osher, S.R. Chakravarthy, *Journal of Computational Physics* 71(2), 231 (1987).
49. G.S. Jiang, C.W. Shu, Efficient implementation of weighted eno schemes. Tech. rep., DTIC Document (1995).
50. J.W. Barrett, J.F. Blowey, H. Garcke, *SIAM Journal on Numerical Analysis* 37(1), 286 (1999).
51. C.M. Elliott, S. Larsson, *Mathematics of Computation* 58(198), 603 (1992).
52. D. Kay, R. Welford, *Journal of Computational Physics* 212(1), 288 (2006).
53. R.D. Travasso, M. Castro, J.C. Oliveira, *Philosophical Magazine* 91(1), 183 (2011).
54. R.D. Travasso, E.C. Poiré, M. Castro, J.C. Rodriguez-Manzaneque, A. Hernández-Machado, *PLoS one* 6(5), e19989 (2011).
55. T. Belytschko, S. Loehnert, J.H. Song, *International Journal for Numerical Methods in Engineering* 73(6), 869 (2008).
56. S. Zhang, S.L. Mielke, R. Khare, D. Troya, R.S. Ruoff, G.C. Schatz, T. Belytschko, *Physical Review B* 71(11), 115403 (2005).
57. W.K. Liu, S. Hao, T. Belytschko, S. Li, C.T. Chang, *International Journal for Numerical Methods in Engineering* 47(7), 1343 (2000).
58. M. Tawhai, J. Bischoff, D. Einstein, A. Erdemir, T. Guess, J. Reinbolt, *Engineering in Medicine and Biology Magazine*, *IEEE* 28(3), 41 (2009).
59. D.A. Nordsletten, B. Yankama, R. Umeton, V. Ayyadurai, C. Dewey, *Biomedical Engineering*, *IEEE Transactions on* 58(12), 3508 (2011).
60. J. Zhou, I.F. Thorpe, S. Izvekov, G.A. Voth, *Biophysical journal* 92(12), 4289 (2007).
61. S.C. Flores, J. Bernauer, S. Shin, R. Zhou, X. Huang, *Briefings in bioinformatics* 13(4), 395 (2012).
62. S. Kmieciak, M. Jamroz, A. Kolinski, in *Multiscale Approaches to Protein Modeling* (Springer, 2011), pp. 281–293.
63. N. Bellomo, M. Delitala, *Physics of Life Reviews* 5(4), 183 (2008).
64. P. Hunter, P. Nielsen, *Physiology* 20(5), 316 (2005).
65. P.J. Hunter, E.J. Crampin, P.M. Nielsen, *Briefings in bioinformatics* 9(4), 333 (2008).
66. H. De Jong, *Journal of computational biology* 9(1), 67 (2002).
67. W.K. Liu, E. Karpov, S. Zhang, H. Park, *Computer Methods in Applied Mechanics and Engineering* 193(17), 1529 (2004).